Journal of the Mechanical Behavior of Biomedical Materials 184 (2026) 107630

Contents lists available at ScienceDirect

Journal of the Mechanical Behavior of Biomedical Materials

journal homepage: www.elsevier.com/locate/jmbbm

Electrospun PCL/BG composite scaffolds: processing, optimization and surface modification to improve wettability and cell attachment

Francesco Gerardo Mecca [a], Devis Bellucci [a,*], Alessia Mazzilli [b], Francesco Demetrio Lofaro [b], Daniela Quaglino [b], Valeria Cannillo [a,**]

[a] Department of Engineering "Enzo Ferrari", University of Modena and Reggio Emilia, Via P. Vivarelli 10, Modena, 41125, Italy
[b] Department of Life Sciences, University of Modena and Reggio Emilia, Via G. Campi 287, Modena, 41125, Italy

ARTICLE INFO

Keywords:
Electrospinning
Composite
Bioactive glass
Wettability
Biological tests

ABSTRACT

The design of biomedical devices for tissue engineering has attracted significant research interest since the late twentieth century. Among the available fabrication techniques, electrospinning has emerged as a versatile approach for producing fibrous scaffolds for various applications, such as wound dressing and healing, as well as bone tissue regeneration. In this context, the synergistic use of bioactive glass (BG) has gained significant attention due to its well-established properties including osteogenesis, osteoinduction, angiogenesis, wound healing, soft tissue repair and antibacterial effects. In this work, S53P4_MS, (composition in mol.%: SiO_2 53.8, P_2O_5 1.7, Na_2O 7.7, CaO 21.8, MgO 5, SrO 10), a novel melt-derived composition with remarkable thermal and biological properties, was employed as a powdered ceramic filler in electrospun poly(ε-caprolactone) (PCL) mats. This study focused on optimizing previously developed procedures for producing electrospun PCL/BG scaffolds, with particular attention to overcoming the intrinsically hydrophobic nature of electrospun PCL, which may limit scaffold functionality. To this end, a chemical surface modification treatment based on immersion in a sodium hydroxide (NaOH) solution was integrated into the fabrication process, and the properties of the chemically treated samples were compared with those of the untreated counterparts. Although the NaOH treatment significantly reduced the contact angle, the resulting values (an average reductionin contact angle of 26%) remained close to the hydrophobic/hydrophilic threshold, indicating improved wettability rather than a complete transition to a strongly hydrophilic surface. Furthermore, the adhesion and spreading of osteosarcoma cell lines (Saos-2) and of human dermal fibroblasts (HDFs) on the PCL/BG scaffolds were markedly enhanced by NaOH treatment. This work ultimately aims to contribute to the optimization of particle-loaded electrospun scaffolds, which could have interesting application potentials in hard and soft tissue engineering and tissue repair, aspects that deserve to be further explored.

1. Introduction

Over the past decades, research on biomaterials has increasingly focused on the development and optimization of scaffolds for tissue engineering applications. Scaffolds provide temporary structural support that promotes the regeneration of damaged or missing tissue (Chan and Leong, 2008). Among the various scaffold fabrication techniques employed for both soft and bone tissue engineering, electrospinning has attracted increasing attention (Jun et al., 2018), due to its numerous inherent advantages, such as ease of setup, relatively low material cost, cost-effectiveness, and the wide range of scaffold morphologies and compatible materials (Keirouz et al., 2023). Specifically, electrospinning enables the fabrication of flat, fibrous scaffolds, by subjecting a polymeric solution to a high electrical potential. The solution is fed at a known flow rate through a needle, where the applied electrical potential stretches the viscoelastic fluid into a thin jet. During flight, the solvent evaporates, leading to the formation of polymeric fibers ranging from micro-to nanoscale, which are collected as a nonwoven mat (Jun et al., 2018; Bhardwaj and Kundu, 2010).

One of the most widely employed and studied polymers for electrospinning is poly(ε-caprolactone) (PCL) (Joseph et al., 2019; Chen et al., 2009; Ekaputra et al., 2009), a biocompatible semi-crystalline

* Corresponding author.
** Corresponding author.
E-mail addresses: devis.bellucci@unimore.it (D. Bellucci), valeria.cannillo@unimore.it (V. Cannillo).

https://doi.org/10.1016/j.jmbbm.2026.107630
Received 7 May 2026; Received in revised form 9 July 2026; Accepted 8 September 2026
Available online 9 September 2026

polyester known for its high mechanical properties and tunable biodegradation rate (Woodruff and Hutmacher, 2010; Wei et al., 2018). PCL is often used either in its pure form or blended with other polymers or particulate additives, such as hydroxyapatite (Sattary et al., 2019; Jaiswal et al., 2013; Jirkovec et al., 2021) or bioactive glasses (BGs) (Allo et al., 2010; Tabia et al., 2021; Piatti et al., 2023).

BGs are a class of biomaterials extensively studied in literature due to their remarkable biological properties. They are biocompatible materials (Hench et al., 2004) that, upon implantation, induce the precipitation of a hydroxyapatite layer on their surface, thereby promoting osteogenesis and osteoinduction (Kaur et al., 2014). At the same time, BGs can form a strong chemical bond with bone and, for some compositions, also with soft tissue. Beyond their well-documented bone-regenerative capabilities (Aboelsaad et al., 2008; Fernandes et al., 2018; Jones et al., 2007), BGs can exhibit a wide range of additional properties, such as angiogenesis stimulation, antibacterial activity, or wound healing effects, depending on their composition (Jones, 2013). In particular, the inclusion of certain metallic or alkali ions allows for the tailoring of these properties to elicit targeted biological or mechanical responses (Moghanian et al., 2025; Mecca et al., 2023; Rabiee et al., 2015).

Over the past five decades, numerous BG compositions have been developed, including 45S5 Bioglass® (composition in mol.%: SiO_2 46.1, P_2O_5 2.6, Na_2O 24.4, CaO 26.9), the first commercially available silicate BG, which is still considered a reference composition (Hench, 2006), and S53P4 (composition in mol.%: SiO_2 53.8, P_2O_5 1.7, Na_2O 22.7, CaO 21.8), a more recently developed commercially available formulation with notable biological properties (Lindfors et al., 2010), as well as antibacterial activity (Drago et al., 2014; Coraça-Huber et al., 2014).

The inclusion of ions such as magnesium and strontium in BG compositions has recently been explored (Sergi et al., 2020; Bellucci et al., 2024). Magnesium has been investigated as a BG dopant due to its biological significance, being naturally present in bone and enamel and playing multiple important roles in the body (Kargozar et al., 2022; Cacciotti, 2017; Zreiqat et al., 2002). Moreover, magnesium deficiency has been associated with reduced bone density and an increased risk of osteoporosis (Cacciotti, 2017; Percival, 1999). Strontium, on the other hand, is known to regulate osteoblast and osteoclast activity (Cacciotti, 2017; Bonnelye et al., 2008) and has also been reported to exhibit antibacterial effects (Moghanian et al., 2017; Baheiraei et al., 2021).

S53P4_MS (composition in mol.%: SiO_2 53.8, P_2O_5 1.7, Na_2O 7.7, CaO 21.8, MgO 5, SrO 10) is a novel silicate BG derived from S53P4, in which calcium is partially substituted with magnesium and strontium. In previous studies, its biological properties outperformed those of S53P4 when tested using the 3T3 cell line and human dermal fibroblasts (HDF) (Bellucci et al., 2024). Moreover, its comparatively milder dissolution kinetics could prevent excessive alkalinization of the surrounding biological environment when it comes into contact with the BG.

The utilization of BGs in electrospun scaffolds has received increasing attention in recent years. In fact, researchers have explored both the use of sol-gel-derived BGs as precursor solutions for electrospinning (Nagrath et al., 2019; Lu et al., 2008) and the incorporation of suspended melt-derived particles into polymeric solutions (Shams et al., 2018; Hochleitner et al., 2017). Several studies report that BGs embedded in electrospun fibers retain their bioactivity and ion release, promoting hydroxyapatite precipitation in *in vitro* tests (Liverani et al., 2018; Elkhouly et al., 2021), while maintaining good biocompatibility (Liverani et al., 2018; Elkhouly et al., 2021; Serio et al., 2019). Moreover, BG particle size influences the dissolution kinetics in electrospun mats, as micro-sized particles allow for a more controlled ion release (Serio et al., 2019). However, BG incorporation also presents several challenges. For instance, the addition of BG particles can influence the mechanical properties of the fibrous mats, as higher Young's modulus and lower tensile strength and elongation are reported in the literature (Elkhouly et al., 2021; Serio et al., 2019). Furthermore, the addition of BG into electrospun mats has been reported to increase the average fiber diameter depending on filler morphology and dispersion (Liverani et al., 2018; Konyalı and Deliormanlı, 2019). Lastly, achieving homogeneous dispersion and preventing particle agglomeration are also crucial aspects of the production of these scaffolds (Mecca et al., 2025). Still, BGs are an attractive material for producing electrospun scaffolds capable of exhibiting multiple beneficial biological properties in both soft and hard tissue engineering applications (Lu et al., 2008; Moura et al., 2017; Luginina et al., 2020).

The wettability of electrospun PCL mats represents a crucial challenge in the manufacturing of these kinds of scaffolds. Typically, electrospun PCL mats have a highly hydrophobic surface, resulting in reduced biological performance, limited cell adhesion, and decreased protein adsorption (Kim et al., 2006; Tiyek et al., 2019). This can negatively affect the scaffold's functionality and limit its applicability in clinical settings. To address this issue, different strategies have been proposed, such as plasma treatment or functionalization by immersion in a sodium hydroxide (NaOH) solution (Bosworth et al., 2019; Yaseri et al., 2023). Among these approaches, chemical treatment in NaOH can be considered an accessible and practical solution for several reasons, including high availability of reagents, low cost, and ease of implementation. Increasing the hydrophilicity of these devices could significantly enhance their biological performance, providing valuable tools for various applications, such as skin tissue healing, infection control, and BG delivery for bone regeneration (Bosworth et al., 2019; Yaseri et al., 2023).

To date, relatively few studies have investigated the incorporation of melt-derived particulate BGs into electrospun PCL-based scaffolds, especially in combination with surface modification strategies to increase wettability. Such systems pose potential applications not only in the area of bone tissue engineering, but also for soft tissue repair. Moreover, the inclusion of Mg- and Sr-doped BG may introduce additional biological effects due to the known role of these ions in modulating cellular activity and tissue regeneration. The aim of this work was to investigate the feasibility of electrospun PCL/S53P4_MS scaffolds, building on established fabrication methods reported in previous work (Mecca et al., 2025). The study focuses on a comparative evaluation of different composite scaffold formulations fabricated under similar electrospinning conditions, in order to isolate the influence of bioactive glass. Firstly, BG incorporation efficiency was considered a crucial aspect of the electrospinning process. Subsequently, the effects of chemical surface modification treatment in NaOH on scaffold wettability and mechanical behavior were evaluated by testing the mats both before and after treatment. This was done to address key issues of this type of electrospun mat, such as highly hydrophobic behavior, low BG incorporation efficiency, and limited mechanical performance. In addition, the biological properties of the electrospun mats were investigated before and after chemical surface modification in NaOH, through cell adhesion tests and the evaluation of cell morphology. In fact, NaOH surface modification could enhance scaffold wettability and, consequently, improve cell attachment in the resulting PCL/BG composite systems.

2. Materials and methods

2.1. Production of PCL/BG electrospun scaffolds

The S53P4_MS BG was manufactured using a traditional melt-quench technique. Raw carbonates and silica (acquired from Carlo Erba Reagents S.r.L, Rodano, Italy) were weighed and mixed for 4 h. The powder mix was then decarbonized at 1100 °C for 1 h and melted at 1450 °C in a laboratory furnace. The molten mass was subsequently quenched in room-temperature water and dried in a heater at 110 °C overnight, obtaining a glass frit. The BG frit was ground into a powder via dry milling for 20 min, using an alumina jar and a laboratory mill MGS1800/2 (MGS S.r.l., Fiorano Modenese, Italy), then sieved to a powder with granulometry <63 μm. The BG powder underwent a

Table 1
Compositions of the suspensions used to manufacture electrospun samples.

	SP_H	SP_L	SP_X
DCM	6.5 mL	6.5 mL	6.5 mL
DMF	3.5 mL	3.5 mL	3.5 mL
PCL	0.90 g	0.90 g	1.00 g
S53P4_MS	0.27 g	0.135 g	0.3 g
Nominal PCL/BG weight ratio	23%	13%	23%

Table 2
Electrospinning parameters employed in the production of samples.

	SP_H	SP_L	SP_X
Applied voltage	12 kV	11.5 kV	13.5 kV
Negative voltage	−5 kV	−5 kV	−5 kV
Flow rate	2.4 mL/h	2.4 mL/h	2.4 mL/h
Needle-collector distance	15 cm	15 cm	15 cm
Scanning emitter speed	25 mm/s	25 mm/s	25 mm/s
Rotating collector speed	250 rpm	250 rpm	250 rpm
Total electrospun volume	5 mL	5 mL	5 mL

second, wet milling in ethanol (EtOH) for 1 h, using a BG:EtOH:balls weight ratio of 1:20:20. The BG/EtOH suspension was allowed to decant, the supernatant was removed, and the remaining wet slurry was dried in a ventilated oven at 50 °C for 48 h.

Electrospun scaffolds were manufactured using an electrospinning machine Spinbox® (Bionicia, Valencia, Spain), equipped with a rotating collector, syringe pump, negative voltage generator, and scanning emitter. The mats were prepared starting from a BG suspension in a PCL solution. The appropriate amount of S53P4_MS was weighed and placed into a glass vial. 3.5 mL of Dimethylformamide (DMF) were added into the vial, which was then sonicated for 10 min. The appropriate amount of PCL (MW~80.000, acquired from VWR International S.r.L., Milano, Italy) was weighed and added to the vial together with 6.5 mL of Dichloromethane (DCM). These solvents were chosen as DCM can easily dissolve PCL, while DMF, due to its higher dielectric constant, stabilizes the jet (Du et al., 2016). The solvent ratio was chosen based on previous experimentation with different solutions. Lastly, the suspensions were stirred overnight at room temperature and at a speed of 500 rpm.

The detailed compositions of the suspensions for each formulation are reported in Table 1. Three formulations were prepared in order to investigate the effect of BG loading on the electrospun scaffolds. The sample SP_H represents an intermediate composition, with a nominal BG content of 23.08 wt% relative to the total solid phase. The formulation SP_L was prepared with a lower BG content (13.04 wt%), while SP_X contained higher amounts of both PCL and BG compared to SP_H, maintaining the same nominal BG fraction (23.08 wt%). The selected BG contents are consistent with values commonly reported in the literature for electrospun polymer/BG composites, as excessively high inorganic filler loading may alter electrospinnability and compromise fiber formation (Konyalı and Deliormanlı, 2019; Luginina et al., 2020; Kouhi et al., 2013). Moreover, these BG concentrations are consistent with the range commonly adopted for electrospun PCL/BG composites and have been reported to provide a good balance between biological performance and processability in polymer/BG composite scaffolds (Gerhardt and Boccaccini, 2010). Prior to electrospinning, the suspensions were sonicated for an additional 5 min, then poured into a syringe and electrospun through a 17 G needle (internal diameter Φi = 1.067 mm). The electrospinning parameters for each sample are reported in Table 2. In brief, the total voltages employed were between 16.5 and 18.5 kV, while the flow rate and needle-collector distance were constant at 2.4 mL/h and 15 cm, respectively.

2.1.1. Treatment of PCL/BG scaffolds in NaOH solution

In order to increase the wettability of the electrospun scaffold, aiming to improve its biological properties and better exploit the properties of BG, the samples, following procedures reported in the literature (Bosworth et al., 2019), were chemically treated in a 1M NaOH solution made of NaOH pellets (Incofar S.r.L., Modena, Italy) in Milli-Q bi-distilled water. Samples were secured onto a Petri dish and submerged in the NaOH solution at room temperature for 4 h. The samples were then collected, washed with bi-distilled water, and dried at room temperature for 24 h. The treated samples were named accordingly SP_HT, SP_LT, and SP_XT, and characterized as follows.

2.2. Characterization

2.2.1. BG powder characterization

Properties of S53P4_MS, including biological ones, have already been investigated elsewhere (Bellucci et al., 2024). To increase the stability of the suspension during the electrospinning process, and improve the quality of the fibers, BG particles should have a fine particle size (Serio et al., 2019). The granulometry of the powders, both sieved after the first milling step and after re-milled, was verified using a laser-diffraction particle size distribution analyzer (Malvern Panalytical, Malvern, UK). Moreover, the powders were observed under Field-Emission Scanning Electron Microscope (SEM) (Fei Quanta 200, Thermo-Fisher Scientific, Waltham, MA, USA) equipped with both a secondary electron detector and a backscattered electron detector working simultaneously. The micrographs were acquired at a magnification of 1600×. The characteristic diameters $D_{0.1}$, $D_{0.5}$, and $D_{0.9}$, corresponding to the particle diameters below which 10%, 50%, and 90% of the particle population are found, respectively, are reported along with the particle size reduction (PSR), calculated as:

$$PSR = \frac{(D_s - D_d)}{D_s} \times 100\%, \quad (1)$$

where D_s is the mean diameter after single milling, and D_d is the mean diameter after the second milling.

2.2.2. Thermogravimetric analysis

Thermogravimetric analysis (TGA) was conducted on the electrospun samples to quantify the effective electrospinning yield of BG. The analysis was carried out by heating the samples to a temperature sufficient to ensure complete thermal degradation of the polymeric phase (PCL), while remaining below the temperature range at which thermal reactions of BG occur. Small samples weighing 15 ± 4 mg were cut from the electrospun mat, and placed in a simultaneous thermal analyzer STA 429 CD (Netzsch GmbH, Selb, Germany). A heating rate of 20 K/min was applied up to a temperature of 600 °C in an air atmosphere; this temperature was selected considering the high thermal stability of S53P4_MS up to 700 °C (Bellucci et al., 2024).

2.2.3. SEM-EDS analysis

The electrospun mats were characterized using a field-emission SEM (Fei Quanta 200, ThermoFisher Scientific, Waltham, MA, USA), equipped with a secondary electron detector. Images of the sample surfaces were acquired at magnifications of 3000× and 5000×. Small 0.5 × 0.5 cm patches were cut from the mats and sputter-coated with a 10 nm gold layer. Moreover, Energy-dispersive X-ray spectroscopy (EDS; Quantax 200, Bruker Corp., Billerica, MA, USA) was used to verify the presence and spatial distribution of S53P4_MS within the electrospun fibers via elemental mapping. SEM micrographs were subsequently used to determine the mean diameter of the fibers using the open-source image analysis software ImageJ (version 1.54d, NIH, Bethesda, MD, USA). The 5000× magnification micrographies were employed to measure the fiber diameter. At least 50 measurements were taken on each sample. Mean fiber diameter and standard deviation were thus calculated. A one-way analysis of variance (ANOVA) with Tukey's post-test was performed on the fiber diameter data. Statistical significance was set at $p < 0.05$.

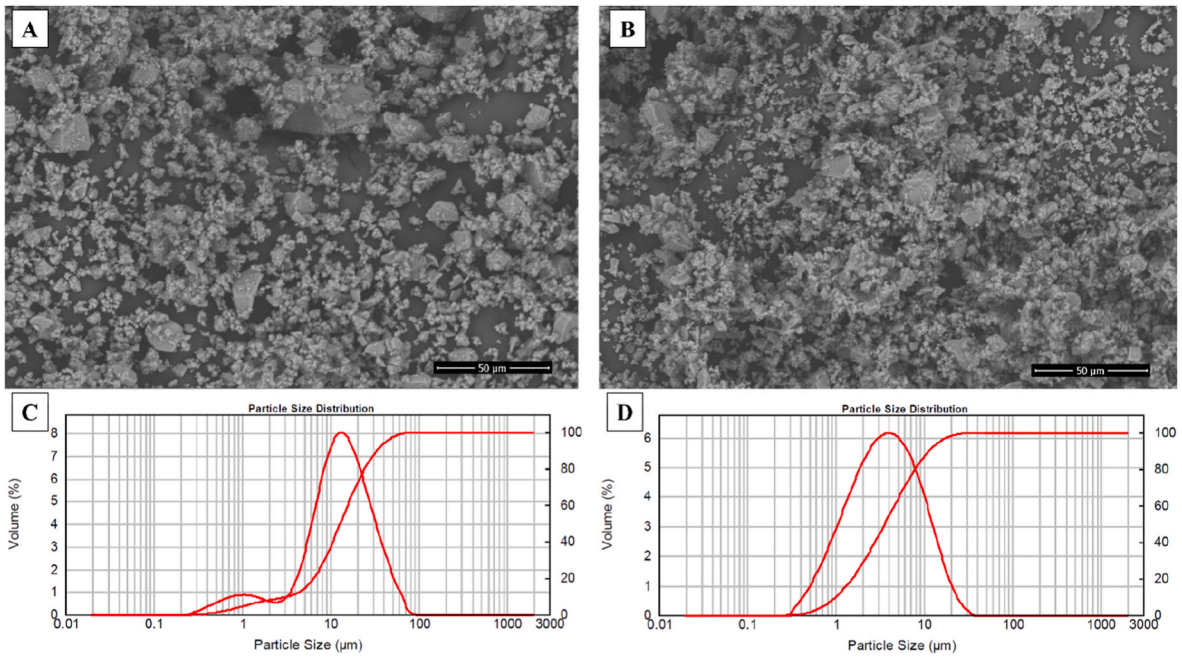

Fig. 1. SEM micrographs of the S53P4_MS powders after the initial milling (A) and after the second milling (B), and their corresponding cumulative and differential distribution for the single- (C) and double-milled (D) powder.

2.2.4. Water contact angle

Water contact angles of the electrospun samples were measured using an automatic optical contact angle system (OCA 15 EC, Data-physics Instruments GmbH, Stuttgart, Germany) equipped with a 6.5× zoom lens. The measurements were conducted on samples both untreated and after treatment in NaOH in order to compare the wettability of treated and untreated samples. Small 5 × 2 cm strips were cut from the samples and secured to a flat dish. Droplets of 2 µL were dispensed on the surfaces and, after waiting 5 s, both right and left angles were measured digitally (SCA 20, DataPhysics Instruments GmbH, Germany). At least 10 measurements were acquired for each sample. The collected data were then used to calculate the mean contact angle for the samples' surfaces. A two-way ANOVA analysis for unbalanced data ($\alpha = 0.05$, variable A: sample type, variable B: treatment condition) was conducted to evaluate the variance of the results, particularly with respect to chemical treatment. For the sake of clarity, the resulting data include the contact angle reduction factor (RCA) calculated as:

$$R_{CA} = \frac{\theta_{ut} - \theta_t}{\theta_{ut}} \times 100\%, \quad (2)$$

where θ_{ut} is the mean contact angle of the untreated samples and θ_t is the contact angle of the treated samples, employed to quantify the variability in contact angle measurements.

2.2.5. Mechanical properties

Prior to tensile testing, the thickness of each mat was measured in the vicinity of the area from which the tensile samples were collected. Optical imaging was used to determine the mean thickness of the electrospun mat, thanks to the improved thickness uniformity achieved via the scanning-emitter-assisted electrospinning process. 0.5 × 0.5 cm patches of electrospun samples were cut from the mat from zones adjacent to those used for tensile tests. These small patches were secured between two semi-rigid supports and embedded in cold-curing resin. After 24 h of curing, the resin was sectioned and polished; the cross-sections were examined under an optical microscope (Olympus Corp., Tokyo, Japan) at 500× magnification. The mean thickness of the samples was subsequently measured using ImageJ (version 1.54d).

The ultimate tensile strength (σ_{MAX}), elongation at failure (ε_b), and Young's Modulus (E) were obtained using a universal testing machine (Z050, Zwick-Roell GmbH & Co. KG, Ulm, Germany) equipped with a 10 kN load cell (XForce HP, Zwick-Roell). Samples were cut into 20 × 15 mm strips along the longitudinal direction, defined as parallel to the radial component of the collector cylinder's velocity, and secured onto custom-made polylactic acid grips. A preload of 0.2 N was applied to the samples, and the test was conducted at a speed of 5 mm/min, ultimately bringing the samples to failure. At least 5 repetitions were conducted for each sample. The data collected were then used to calculate the mean values of the samples' σ_{MAX}, ε_b and E. The modulus was determined from the stress–strain response over an elongation range of 2% to 4%, which falls fully within the elastic region for all samples. A one-way analysis of variance was conducted on the samples to determine statistically significant differences among the scaffold formulations and treatments. Additionally, representative stress–strain curves are shown to qualitatively illustrate the mechanical response of untreated and treated scaffolds.

2.3. Biological tests: cell attachment and spreading

Prior to cell seeding, the PCL/BG scaffolds were sterilized by incubation in 70% ethanol for 30 min followed by three washes with Dulbecco's Phosphate-Buffered Saline (DPBS, ThermoFisher Scientific, MA, USA). Saos-2 cells, a widely used osteosarcoma cell line (Cat. CLS-300331, Cytion) and human dermal fibroblasts (HDF, Cat. #C-013-5C, ThermoFisher Scientific), at the concentration of 1.0×10^4 cells were suspended in 1 mL of Minimum Essential Medium (MEM) or Dulbecco's Modified Eagle Medium (DMEM) for Saos-2 and HDF, respectively. Both media were supplemented with 10% fetal bovine serum, 1% penicillin-streptomycin and 1% non-essential amino acids (Thermo Fisher Scientific). 1 mL of this suspension was placed onto each scaffold cut to have the same surface area (1 cm^2) for the same number of cells. Scaffolds were placed on non-treated cell-culture plates for 1 h to let cells adhere to the scaffold. Then, each scaffold was transferred into 24-well cell culture plates (Corning, NY, USA) and incubated at 37 °C with 5% CO_2 in complete MEM or DMEM. After the transfer, there were no cells left on the culture plates. After 24 h, all samples were fixed with 4% paraformaldehyde for 15 min.

Table 3
Results of the granulometric analysis on S53P4_MS powders after a single and double milling process, expressed as $D_{0.1}$, $D_{0.5}$, and $D_{0.9}$ (in μm), and PSR values.

	$D_{0.1}$	$D_{0.5}$	$D_{0.9}$
Single milling	3.34	12.86	33.40
Double milling	1.00	3.57	11.22
PSR	70%	72%	66%

Fluorescent markers were used to boost the visualization of cells and their morphology on the scaffolds. Briefly, cells were permeabilized with 0.5% Tween-20 in DPBS for 10 min and then incubated for 5 min with 300 nM DAPI (D1306, ThermoFisher Scientific) and for 45 min with iFluor-488-conjugated phalloidin (1:1000 dilution, ab176753, Abcam, UK), to stain the nuclei and the actin cytoskeleton, respectively. Samples were then washed with DPBS and observed with a 20× Olympus objective mounted on an EVOS M5000 (ThermoFisher Scientific).

To quantify the number of cells attached and grown on the scaffolds, nuclei/unit area were counted using the ImageJ software (v.1.53t) on 10 images from each sample taken randomly at 10× magnification on the whole surface of the scaffolds. Experiments were performed in duplicate. One-way ANOVA was used for multiple comparisons and a Tukey post-hoc test was applied. Statistical analyses were performed using GraphPad Prism 8.0 software (San Diego, CA, USA). Values are reported as mean ± standard deviation. Differences were considered significant for $p < 0.05$.

3. Results and discussion

3.1. Morphological and compositional characterization of electrospun PCL/BG scaffolds

S53P4_MS underwent a double milling process to ensure a fine particle size of the powders. This approach was followed to minimize BG sedimentation during electrospinning, which can lead to reduced BG incorporation in the final product compared to the nominal weight ratio. Furthermore, reducing the maximum particle diameter also decreases the risk of clogging the tubing and needle.

Fig. 1(A and B) presents the SEM micrographs of the S53P4_MS powder after the initial milling and sieving process, and after the subsequent wet milling process. The cumulative and differential particle size distributions obtained from the granulometric analysis are presented in Fig. 1(C and D). Meanwhile, Table 3 reports the characteristic diameters $D_{0.1}$, $D_{0.5}$, and $D_{0.9}$, and the particle size reduction. Results show a sharp reduction in particle size following the wet milling step. Specifically, the median diameter $D_{0.5}$ decreased from 12.86 μm to 3.57 μm, while $D_{0.1}$ and $D_{0.9}$ decreased from 3.34 μm to 1.00 μm and from 33.40 μm to 11.22 μm, respectively. Overall, the particle size reduction was approximately 70% across the characteristic diameters, confirming the effectiveness of wet milling in refining the BG powder. This creates conditions for more stable electrospinning, reducing the risk of sedimentation and clogging.

The surface and fiber morphology of the electrospun PCL/BG scaffolds before and after chemical treatment were investigated by SEM

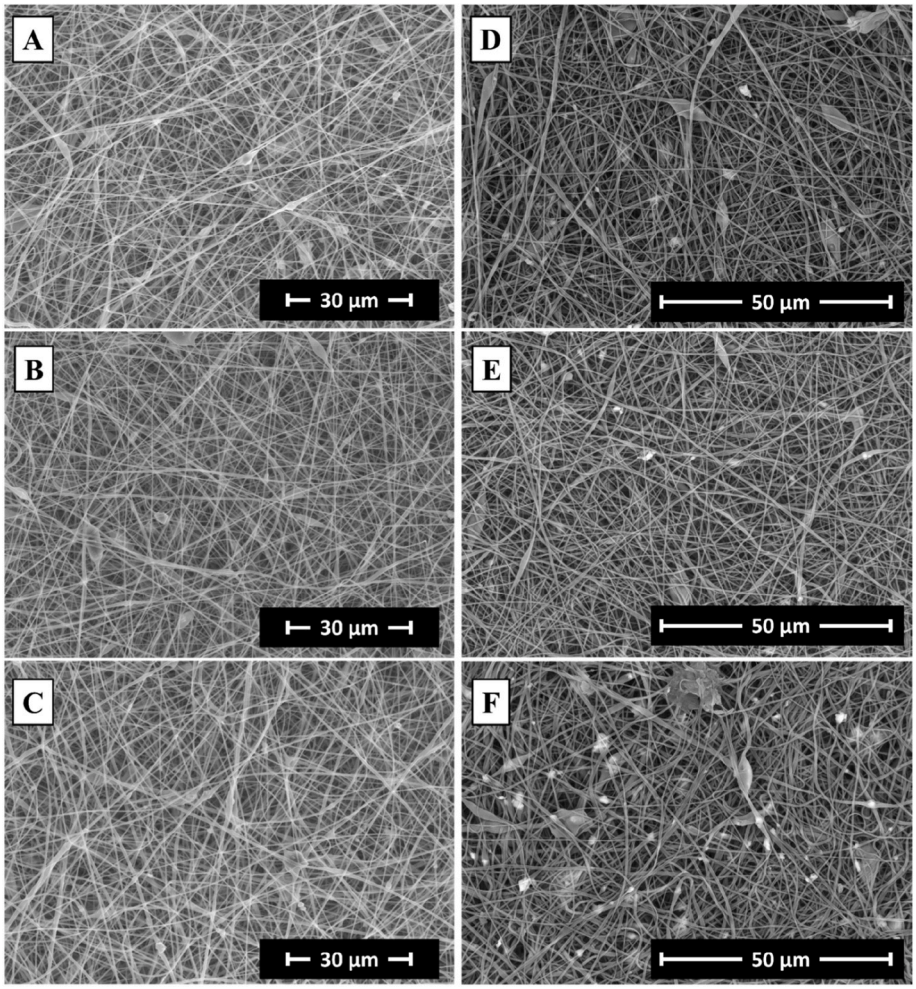

Fig. 2. SEM micrographs of the untreated SP_H (A), SP_L (B) and SP_X (C) samples; and chemically treated SP_H (D), SP_L (E) and SP_X (F) samples.

Table 4
Mean fiber diameter and standard deviation of the electrospun samples. One-way ANOVA and Tukey's post-test showed statistically significant differences between samples SP_H and SP_X ($p < 0.05$).

	SP_H	SP_L	SP_X
Mean fiber diameter	0.376 ± 0.10 μm	0.390 ± 0.12 μm	0.423 ± 0.14 μm

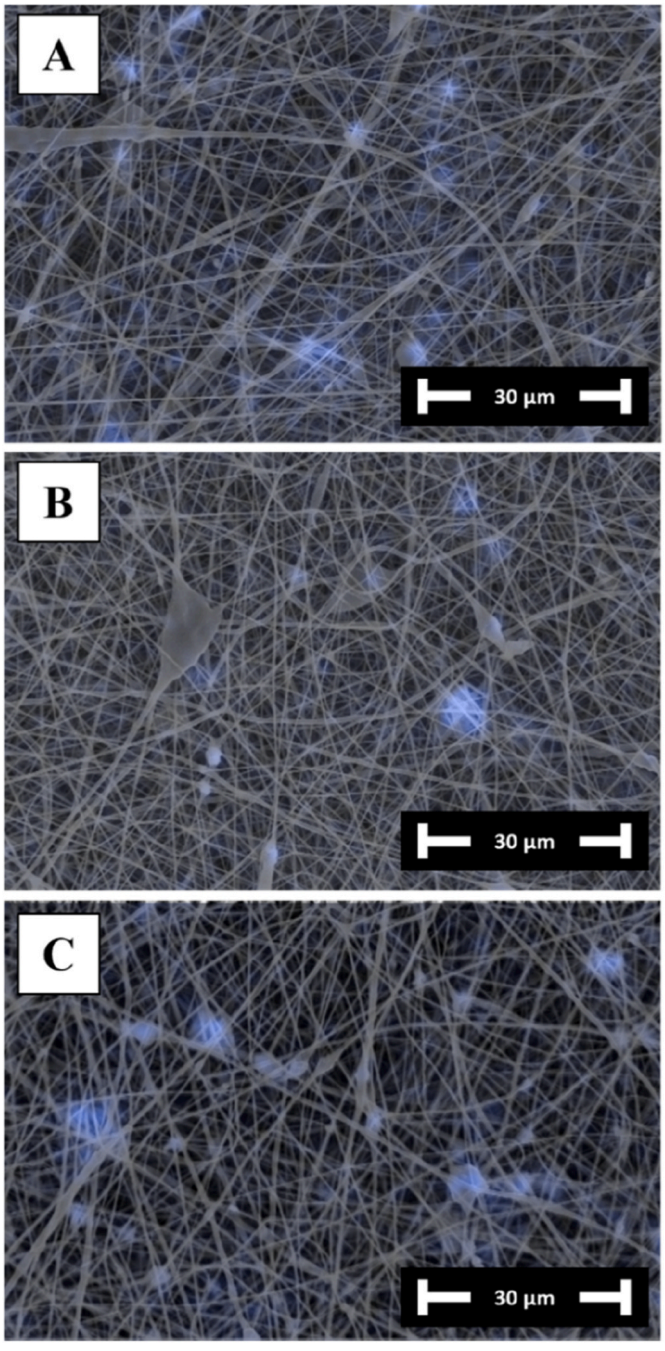

Fig. 3. EDS maps of the untreated electrospun samples SP_H (A), SP_L (B), and SP_X (C). Blue highlighted areas indicate the presence of BG particles. (For interpretation of the references to colour in this figure legend, the reader is referred to the Web version of this article.)

imaging, and the results are reported in Fig. 2. The micrographs show successful electrospinning of the suspensions, with BG particles predominantly embedded within the fibers. SEM analysis also revealed the presence of beads, a morphological defect of the mats consisting of localized fiber thickening (Hong et al., 2016), likely linked to flow fluctuations caused by the suspended BG powders (Hong et al., 2016). Moreover, chemical treatment did not cause any visible morphological alterations to the fibers. SEM micrographs were further employed to measure the mean fiber diameter, and the results are reported in Table 4. Notably, the BG particles are in the micrometer size range, while the electrospun fibers exhibit diameters in the nanometric range. This dimensional mismatch suggests that BG particles are not fully encapsulated within the polymeric matrix; instead, they are likely to induce localized bulges along the fibers (unavoidable in these conditions). However, this could prove useful as direct contact between BG particles and physiological fluids is required to promote ion release and fully exploit the dissolution-related properties of bioactive glasses.

One-way ANOVA revealed a statistically significant difference among the samples ($p = 0.019$). Tukey's post-test identified a significant difference between samples SP_H and SP_X, while no significant difference was detected between SP_L and SP_H, or SP_L and SP_X. Notably, SP_L, characterized by a lower nominal BG content compared to the other samples, did not exhibit a markedly different mean fiber diameter, suggesting that variations in BG loading within the investigated range do not strongly affect the fiber diameter. Furthermore, EDS maps (Fig. 3) were acquired on untreated samples to detect silicon atoms, indicative of the presence of BG. The results further confirmed the presence and homogeneous spatial distribution of BG within the electrospun fibrous mats.

Thermogravimetric analysis was employed to quantify the effective BG content in the electrospun mats, compared to the nominal values. Results are reported in Fig. 4 and summarized in Table 5. TGA revealed that the actual BG content was lower than the nominal value. This was expected, as incorporating insoluble powders as a load during electrospinning is commonly associated with reduced loading efficiency in the final product (Liverani et al., 2021; de Souza et al., 2024). Across all electrospun samples, the retained BG content ranged between 66% and 72% of the nominal value. These values are consistent with previously reported results in the literature (Liverani et al., 2021) and represent an improvement over previous results (Mecca et al., 2025). The enhanced efficiency observed in this work can reasonably be attributed to the modified procedures, including tuning of the electrospinning setup and parameters, as well as the optimized particle size achieved through wet milling. Future efforts could focus on further increasing BG electrospinning efficiency by refining particle dispersion and minimizing sedimentation during manufacturing.

3.2. *Wettability and mechanical behavior of electrospun scaffolds*

The effect of chemical treatment in 1M NaOH solution for 4 h on the surface wettability of the PCL/BG scaffolds was evaluated by measuring and comparing the water contact angle of treated and untreated samples. Table 6 summarizes these results, indicating the mean contact angle and standard deviation of the treated and untreated samples, as well as the RCA. The untreated electrospun mats showed mean contact angles ranging between 119° and 123°, confirming the highly hydrophobic nature of electrospun PCL. Meanwhile, the surface of the chemically treated mats exhibited less hydrophobic behavior, with contact angles ranging from 86° to 94°. While these values still reflect the fact that the surfaces of the mats might be hydrophobic (close to the hydrophobic/hydrophilic threshold), the substantial reduction in contact angle suggests that NaOH treatment can effectively enhance the scaffold's wettability.

Two-way ANOVA for unbalanced data revealed a highly significant main effect of the NaOH treatment on surface wettability ($p \ll 0.05$), independently of scaffold formulation ($p = 0.629$), suggesting that the effect of NaOH treatment was consistent across all scaffold formulations. Notably, the treated samples showed higher dispersion of measurements compared to the untreated samples. This could be attributed to the

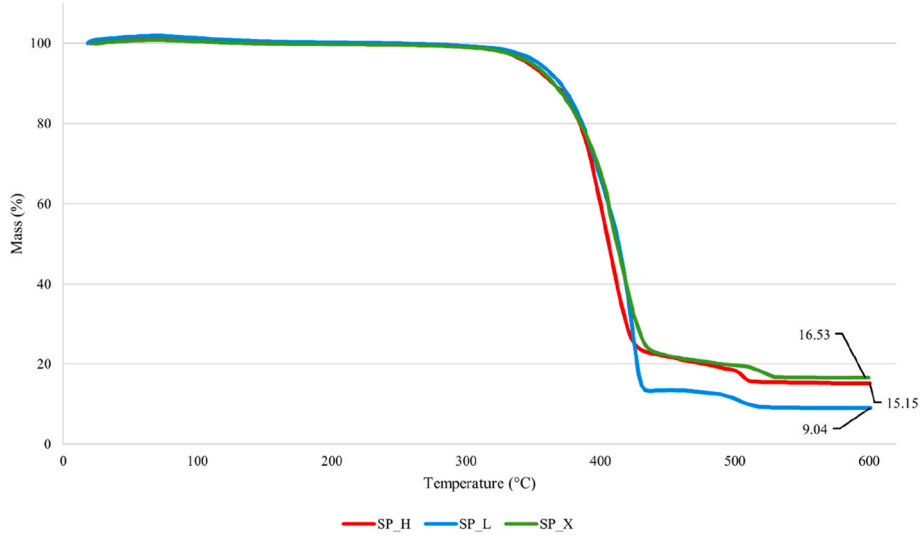

Fig. 4. TGA curves of the electrospun PCL/BG scaffolds, showing polymer degradation and residual BG content.

Table 5
Nominal and measured BG content of the untreated electrospun scaffolds and relative electrospinning efficiency.

	Measured BG content (wt.%)	Nominal BG content (wt.%)	Yield
SP_H	15.15	23	66%
SP_L	9.04	13	69%
SP_X	16.53	23	72%

Table 6
Mean contact angle and standard deviation of the treated and untreated samples, and RCA expressed as percentage.

	mean contact angle (°)	RCA
SP_H	118.88 ± 4.8	28%
SP_HT	85.96 ± 9.9	
SP_L	122.74 ± 4.5	24%
SP_LT	93.52 ± 5.1	
SP_X	121.45 ± 4.4	26%
SP_XT	89.40 ± 11.2	

improved local absorption of water in specific regions of the fibrous structure. This result could be related to surface modification of the scaffolds, which is known to be induced by NaOH treatment of PCL. These results are in accordance with previous findings and further confirm the effectiveness of NaOH treatment on the surface wettability of hydrophobic electrospun PCL (Bosworth et al., 2019; Yaseri et al., 2023).

The mechanical properties of the electrospun PCL/BG scaffolds were evaluated via tensile testing and summarized in Table 7. Moreover, Fig. 5 shows the results of the tests, expressed as mean values of ultimate tensile stress and elongation at break. In addition, Fig. 6 presents exemplary engineering stress–strain curves of samples SP_H and its chemically treated counterpart, SP_HT, providing a qualitative comparison of their mechanical response. Exemplary engineering stress–strain curves obtained from tensile testing of the untreated and treated electrospun scaffolds are provided in the Supplementary Materials.

Overall, the mechanical properties of these scaffolds were improved compared to those reported in previous works (Mecca et al., 2025). This could be generally attributed to the finer fiber diameter achieved in the present work, which has been previously associated with improved mechanical performance in electrospun fibrous mats (Wong et al., 2008; Kim et al., 2016). Untreated scaffolds exhibited tensile strength values in the range of 3–6 MPa, while the treated samples showed higher tensile strength values between 6 and 9 MPa. A similar trend was observed for the ultimate strain, which ranged from 130 to 170% for untreated scaffolds and increased to 140–190% after surface treatment. The results for tensile strength fall within the range typically reported for electrospun PCL-based composite scaffolds, while maintaining relatively high elongation at break (Moura et al., 2017; Luginina et al., 2020). Moreover, samples SP_L and SP_LT clearly exhibited higher tensile resistance compared to other formulations, which could be ascribable to lower BG content, as higher filler content could be associated with reduced mechanical strength in composite electrospun scaffolds (Liverani et al., 2018).

The influence of BG content on the mechanical response of electrospun scaffolds has been widely discussed in the literature. BG nanoparticles embedded into PCL-based fibrous scaffolds can initially increase tensile strength due to a reinforcing effect of the ceramic phase, although higher BG concentrations may lead to a reduction in strength (Kouhi et al., 2013). Several studies point out that excessive inorganic filler in electrospun mats could lead to stress concentration and promote brittle behavior (Piatti et al., 2023; Liverani et al., 2018). Additionally, previous works have highlighted that the mechanical performance of electrospun composites is strongly influenced by the dispersion of BG particles within the polymer matrix. Indeed, poor dispersion and particle clustering may result in localized stress concentration, resulting in worsened mechanical properties (Piatti et al., 2023).

Notably, the mechanical properties of the scaffolds treated in NaOH solution were higher than those of untreated samples, in both elongation

Table 7
Summary of the tensile test results reporting σ_{MAX} (in MPa), E (in MPa) and εb (in %) of the treated and untreated samples as mean ± standard deviation.

	SP_H	SP_L	SP_X	SP_HT	SP_LT	SP_XT
σ_{MAX} (MPa)	3.7 ± 0.4	6.1 ± 0.9	4.0 ± 0.9	6.6 ± 0.4	9.4 ± 1.4	6.3 ± 1.2
ε_b (%)	130 ± 21	174 ± 23	139 ± 52	195 ± 18	166 ± 19	142 ± 38
E (MPa)	9.0 ± 1.0	11.8 ± 1.3	9.0 ± 0.7	10.7 ± 0.4	20.1 ± 2.7	14.6 ± 1.4

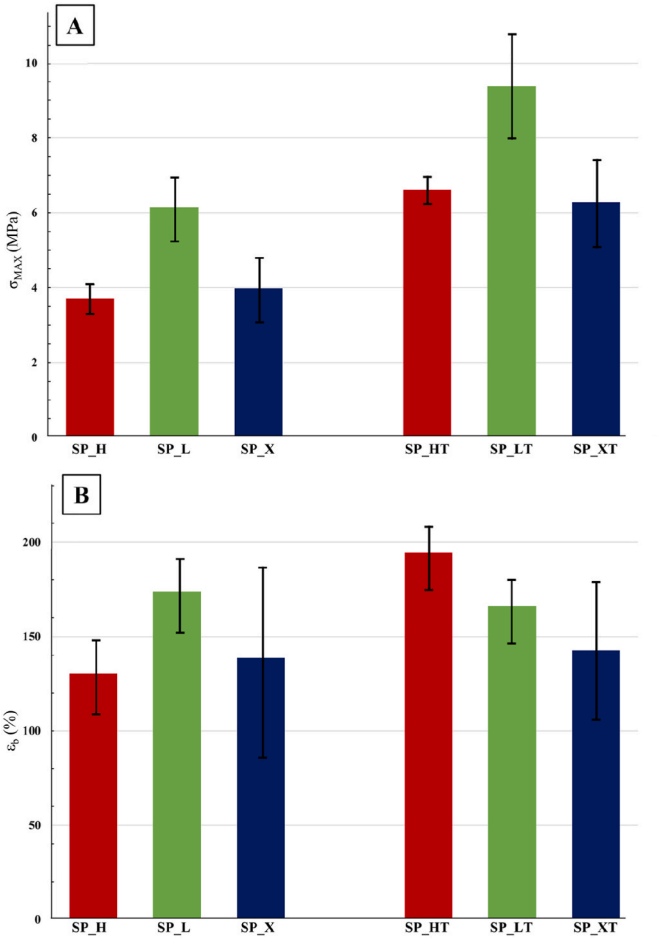

Fig. 5. Tensile test results reporting σ_{MAX} (expressed in MPa) and εb (%) of the treated and untreated electrospun PCL/BG samples.

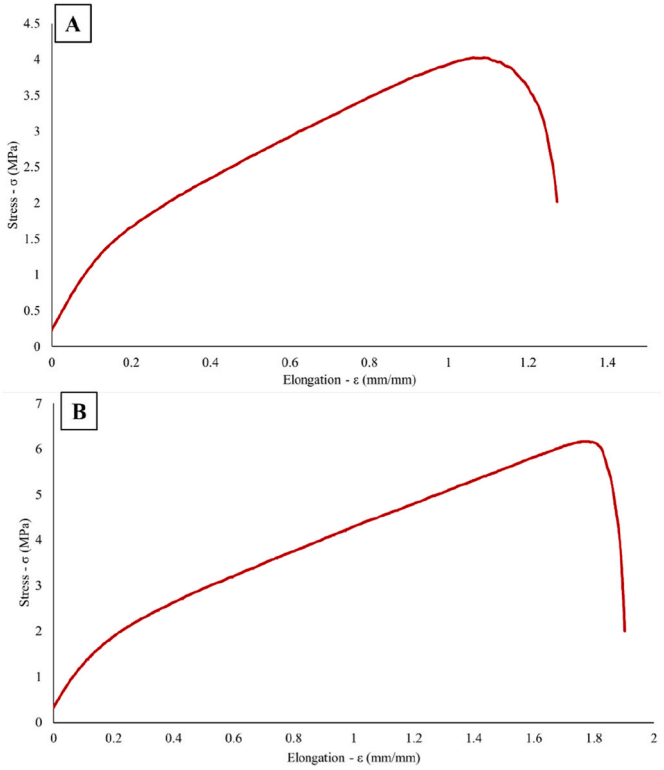

Fig. 6. Representative engineering stress-strain curves of the samples SP_H (A) and the chemically treated SP_HT (B). An additional comparison with engineering stress-strain curves of the samples SP_L and SP_X are available in the Supplementary Materials.

at break and ultimate tensile strength. This could be associated with the chemical treatment, although the underlying mechanisms governing this behavior are not fully elucidated. One-way ANOVA supports the fact that the treated samples exhibit generally higher σ_{MAX}, revealing statistically significant differences among the samples ($F = 15.32$, $p \ll 0.05$). Tukey's post-test revealed a significant increase of tensile strength between treated and untreated samples, except for SP_X compared with SP_XT ($p = 0.17$). Interestingly, statistical analysis revealed the influence of BG loading in the scaffolds, as SP_L shows significantly higher tensile strength compared to SP_H ($p < 0.05$), indicating that lower BG content leads to higher tensile strength in electrospun scaffolds. In contrast, statistical analysis performed on ε_b did not reveal significant differences among the investigated groups ($F = 2.148$, $p = 0.108$). Although variations in elongation at break were observed among the samples, these differences can be attributed to experimental variability rather than systematic effects related to scaffold composition or chemical treatment.

Nevertheless, these results suggest that NaOH treatment, when applied to randomly oriented electrospun fibers for up to 4 h, does not compromise the mechanical performance of the fibrous scaffolds. Cues for this behavior have previously been presented by Bosworth et al., even though this is not fully discussed (Bosworth et al., 2019). Based on the available evidence, the improvement in tensile strength of the treated samples, compared to the untreated ones, could be attributed to a combination of factors. Firstly, NaOH immersion might promote localized fiber fusion (Yaseri et al., 2023). Secondly, NaOH treatment has been reported to induce fiber flattening (Bosworth et al., 2019; Yaseri et al., 2023), resulting in thinner scaffolds compared to the untreated samples. This morphological change may have contributed to an apparent increase in tensile properties, as a smaller cross-sectional area influences stress calculations. However, further dedicated investigations would be required to fully understand the underlying mechanisms.

3.3. Biological test

To preliminarily test the affinity of cells to the different electrospun PCL/BG scaffolds, Saos-2 cells (representative of cells from hard connective tissues) and HDF (representative of cells from soft connective tissues) were cultured on SP_H, SP_L, and SP_X scaffolds, untreated or treated with NaOH, for 24 h, a time point that is normally used for the evaluation of cell adhesion and spreading. Saos-2 cells exhibited the globular-like shape typical of osteoblasts and appeared to adhere very efficiently in all experimental conditions (Fig. 7A). In the case of HDF, cells were shriveled and stretched alongside rounder cells on the SP_X scaffold, whereas were elongated and more expanded on all other samples, and especially on those treated with NaOH, indicating higher affinity for these surfaces (Fig. 7C). Fibroblasts were remarkably numerous and interconnected on SP-L scaffolds treated with NaOH (Fig. 7C). In addition to the morphological evaluations of the cellular monolayer, by light microscopy no cells were observed floating in the medium (as sign of cell death) nor were present on the bottom of the culture plate (as sign of low affinity for the scaffolds).

To better evaluate the number of cells on the different scaffolds, the DAPI-stained nuclei were counted per unit area as described in materials and methods. Adhesion of both Saos-2 cells (Fig. 7B) and HDF (Fig. 7D) showed the best results on NaOH treated scaffolds with significant increases on SP_L and SP_X samples, although some differences were observed depending on the cell type. Indeed, osteoblast cells showed similar affinity for both SP_L and SP_X scaffolds, whereas HDF exhibited

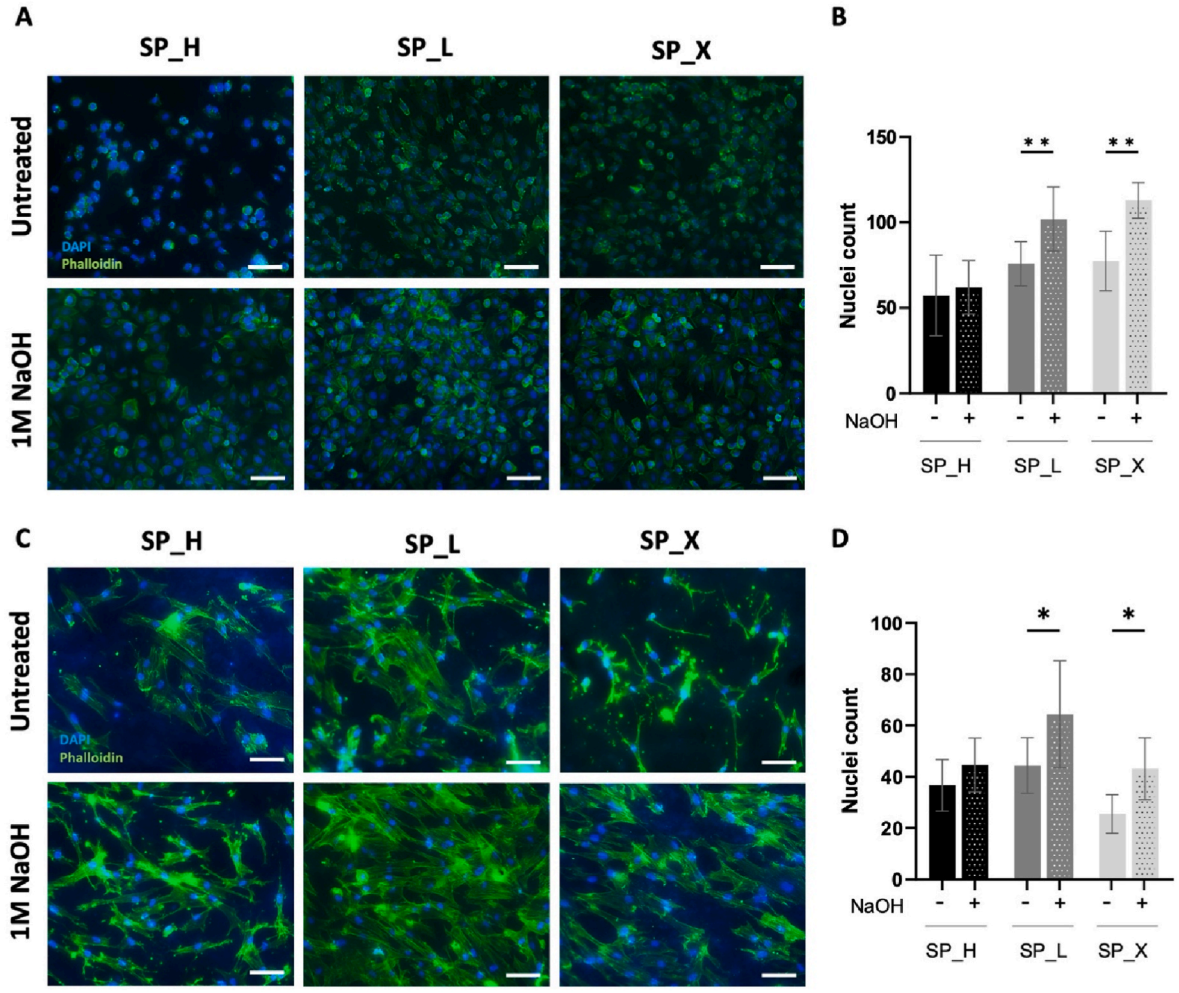

Fig. 7. (**A**) Representative images of osteoblast-like cells (Saos-2) seeded on SP-H, SP-L and SP-X scaffolds untreated or treated with NaOH. Nuclei and cytoskeleton are stained with DAPI (blue) and phalloidin (green), respectively. (**B**) Nuclei count/unit area of Saos-2 seeded on the different scaffolds. (**C**) Representative images of human dermal fibroblasts (HDF) seeded on SP-H, SP-L and SP-X scaffolds untreated or treated with NaOH. Nuclei and cytoskeleton are stained with DAPI (blue) and phalloidin (green), respectively. (**D**) Nuclei count/unit area of HDF seeded on the different scaffolds. Scale bar = 50 μm. Data are shown as mean ± SD. *p value $<$ 0.05, **p *value* $<$ 0.01. (For interpretation of the references to colour in this figure legend, the reader is referred to the Web version of this article.)

a higher number of cells attached to SP-L scaffolds. These differences could be related to the different size and three-dimensional organization of the fibrils within the scaffolds also in relation to the size and shape of cells.

Although further experiments are needed to elucidate a complete spectrum of the different biological properties of the scaffolds, also in terms of cellular differentiation capabilities, overall, these data indicate that the scaffold processing described in this study is suitable for the attachment of cells derived from both hard and soft connective tissues. Moreover, results highlight that alkaline treatment, increasing the wettability of the scaffolds, is associated with improved cell attachment. It can be hypothesized that greater cell adhesion can be mediated by higher adsorption of the serum adhesive glycoproteins present in the culture medium which are indeed known to promote cell adhesion and spreading (Meng et al., 2017).

4. Conclusions

This work showed the feasibility of PCL/S53P4_MS composite electrospun scaffolds, fabricated via the optimization of previously experimented procedures. The implementation of a wet-milling step allowed for high refinement of the powders, improving the electrospinning efficiency. Morphological analyses confirmed the mostly uniform fiber formation (while also presenting beads), and adequate dispersion of the BG in the mats. Moreover, the chemical treatment did not visibly modify the fibers, although NaOH treatment enhanced the wettability of the scaffolds.

The mechanical characterization of the mats showed improved tensile strength compared to previous systems (Mecca et al., 2025). However, it cannot be excluded that differences before and after treatment might be influenced by inaccuracies in the measurements due to sample thinness. Nevertheless, it is feasible to suggest that increased tensile strength is associated with lower fiber diameter that had major influence in this work.

Cellular adhesion and spreading of Saos-2 cells and HDF suggest that NaOH-treated scaffolds exhibited enhanced performances compared to the untreated surfaces, consistently with the improved wettability of the modified surfaces which could be associated with improved protein adsorption from the culture medium. Among the investigated formulations, SP_L exhibited the most favorable cellular response, indicating that both composition and fiber organization might influence interactions between cells and material.

These results indicate that particle size refinement, electrospinning optimization, and surface modification can contribute to improvements in the properties of PCL/BG scaffolds. While a limitation of the present study is the absence of pure PCL scaffolds as reference, which could help

in the determination of the individual contribution of BG incorporation to the wettability, mechanical properties, and response to chemical treatment, these findings provide a basis for the continued development of electrospun composites suitable for both hard and soft tissue engineering and tissue repair applications.

CRediT authorship contribution statement

Francesco Gerardo Mecca: Writing – original draft, Methodology, Investigation, Formal analysis. **Devis Bellucci:** Writing – review & editing, Validation, Methodology, Conceptualization. **Alessia Mazzilli:** Writing – original draft, Investigation, Formal analysis. **Francesco Demetrio Lofaro:** Formal analysis. **Daniela Quaglino:** Writing – review & editing, Validation, Supervision, Funding acquisition. **Valeria Cannillo:** Writing – review & editing, Validation, Supervision, Methodology, Funding acquisition, Conceptualization.

Funding

This research was funded by PNRR MUR project EcosistER Ecosystem for Sustainable Transition in Emilia Romagna ECS_00000033_ECOSISTER (to VC, DQ and FGM) and EcosistER SPIR – Development of an Intelligent Patch for In-situ Biosensing and Restoring Skin Structure and Epidermal Barrier Function (to VC and DQ) .

Declaration of competing interest

The authors declare that they have no known competing financial interests or personal relationships that could have appeared to influence the work reported in this paper.

Appendix A. Supplementary data

Supplementary data to this article can be found online at https://doi.org/10.1016/j.jmbbm.2026.107630.

Abbreviations

The following abbreviations are used in this manuscript

BG	Bioactive Glass
PCL	poly(ε-caprolactone)
NaOH	Sodium hydroxide
HDF	Human Dermal Fibroblasts
EtOH	Ethanol
DCM	Dichloromethane
DMF	Dimethylformamide
PSR	Particle size reduction
SEM	Scanning Electron Microscope
EDS	Energy-dispersive X-ray spectroscopy
TGA	Thermogravimetric Analysis
ANOVA	Analysis of Variance
RCA	Reduction of contact angle
DPBS	Dulbecco's Phosphate-Buffered Saline
DMEM	Dulbecco's Modified Eagle Medium

Data availability

Data will be made available on request.

References

Aboelsaad, N.S., Soory, M., Gadalla, L.M.A., Ragab, L.I., Dunne, S., Zalata, K.R., Louca, C., 2008. Effect of soft laser and bioactive glass on bone regeneration in the treatment of bone defects (an experimental study). Laser Med. Sci. 24 (4), 527–533. https://doi.org/10.1007/S10103-008-0590-Y, 2008, 24.

Allo, B.A., Rizkalla, A.S., Mequanint, K., 2010. Synthesis and electrospinning of ε-Polycaprolactone-Bioactive glass hybrid biomaterials via a sol−Gel process. Langmuir 26, 18340–18348. https://doi.org/10.1021/LA102845K.

Baheiraei, N., Eyni, H., Bakhshi, B., Najafloo, R., Rabiee, N., 2021. Effects of strontium ions with potential antibacterial activity on in vivo bone regeneration. Sci. Rep. 11 (1), 8745. https://doi.org/10.1038/s41598-021-88058-1, 2021, 11.

Bellucci, D., Mazzilli, A., Martelli, A., Mecca, F.G., Bonacorsi, S., Lofaro, F.D., Boraldi, F., Quaglino, D., Cannillo, V., 2024. Enrichment of strontium and magnesium improves the physical, mechanical and biological properties of bioactive glasses undergoing thermal treatments: new cues for biomedical applications. Ceram. Int. 50, 52819–52837. https://doi.org/10.1016/J.CERAMINT.2024.10.135.

Bhardwaj, N., Kundu, S.C., 2010. Electrospinning: a fascinating fiber fabrication technique. Biotechnol. Adv. 28, 325–347. https://doi.org/10.1016/J.BIOTECHADV.2010.01.004.

Bonnelye, E., Chabadel, A., Saltel, F., Jurdic, P.J., 2008. Dual effect of strontium ranelate: stimulation of osteoblast differentiation and inhibition of osteoclast formation and resorption in vitro. Bone 42, 129–138. https://doi.org/10.1016/j.bone.2007.08.043, 2008.

Bosworth, L.A., Hu, W., Shi, Y., Cartmell, S.H., 2019. Enhancing biocompatibility without compromising material properties: an optimised NaOH treatment for electrospun polycaprolactone fibres. J. Nanomater. 2019, 4605092. https://doi.org/10.1155/2019/4605092.

Cacciotti, I., 2017. Bivalent cationic ions doped bioactive glasses: the influence of magnesium, zinc, strontium and copper on the physical and biological properties. J. Mater. Sci. 52 (15), 8812–8831. https://doi.org/10.1007/S10853-017-1010-0, 2017, 52.

Chan, B.P., Leong, K.W., 2008. Scaffolding in tissue engineering: general approaches and tissue-specific considerations. Eur. Spine J. 17, 467. https://doi.org/10.1007/S00586-008-0745-3.

Chen, M., Michaud, H., Bhowmick, S., 2009. Controlled vacuum seeding as a means of generating uniform cellular distribution in electrospun polycaprolactone (PCL) scaffolds. J. Biomech. Eng. 131. https://doi.org/10.1115/1.3173283/400972.

Coraça-Huber, D.C., Fille, M., Hausdorfer, J., Putzer, D., Nogler, M., 2014. Efficacy of antibacterial bioactive glass S53P4 against S. aureus biofilms grown on titanium discs in vitro. J. Orthop. Res. 32, 175–177. https://doi.org/10.1002/JOR.22463.

de Souza, J.R., Cardoso, L.M., de Toledo, P.T.A., Rahimnejad, M., Kito, L.T., Thim, G.P., Campos, T.M.B., Borges, A.L.S., Bottino, M.C., 2024. Biodegradable electrospun PLCL/PEG/Bioactive glass composite scaffold for bone tissue engineering. J. Biomed. Mater. Res. B Appl. Biomater. 112, e35406. https://doi.org/10.1002/JBM.B.35406.

Drago, L., Vassena, C., Fenu, S., De Vecchi, E., Signori, V., Francesco, R. De, Romanò, C. L., 2014. In vitro antibiofilm activity of Bioactive glass S53P4. Future Microbiol. 9, 593–601. https://doi.org/10.2217/FMB.14.20.

Du, L., Xu, H., Zhang, Y., Zou, F., 2016. Electrospinning of polycaprolatone nanofibers with DMF additive: the effect of solution proprieties on jet perturbation and fiber morphologies. Fibers Polym. 17 (5), 751–759. https://doi.org/10.1007/S12221-016-6045-3, 2016, 17.

Ekaputra, A.K., Zhou, Y., Cool, S.M.K., Hutmacher, D.W., 2009. Composite electrospun scaffolds for engineering tubular bone grafts. Tissue Eng. 15, 3779–3788. https://doi.org/10.1089/TEN.TEA.2009.0186.

Elkhouly, H., Mamdouh, W., El-Korashy, D.I., 2021. Electrospun nano-fibrous bilayer scaffold prepared from polycaprolactone/gelatin and bioactive glass for bone tissue engineering. J. Mater. Sci. Mater. Med. 32, 111. https://doi.org/10.1007/s10856-021-06588-6.

Fernandes, H.R., Gaddam, A., Rebelo, A., Brazete, D., Stan, G.E., Ferreira, J.M.F., 2018. Bioactive glasses and glass-ceramics for healthcare applications in bone regeneration and tissue engineering. Materials 11. https://doi.org/10.3390/MA11122530, 2018, 11.

Gerhardt, L.C., Boccaccini, A.R., 2010. Bioactive glass and glass-ceramic scaffolds for bone tissue engineering. Materials 3 (3), 3867–3910. https://doi.org/10.3390/ma3073867. Pages 3867-3910 2010.

Hench, L.L., 2006. The story of bioglass®. J. Mater. Sci. Mater. Med. 17 (11), 967–978. https://doi.org/10.1007/S10856-006-0432-Z, 2006, 17.

Hench, L.L., Xynos, I.D., Polak, J.M., 2004. Bioactive glasses for in situ tissue regeneration. J. Biomater. Sci. Polym. Ed. 15, 543–562. https://doi.org/10.1163/156856204323005352.

Hochleitner, G., Kessler, M., Schmitz, M., Boccaccini, A.R., Teßmar, J., Groll, J., 2017. Melt electrospinning writing of defined scaffolds using Polylactide-Poly(Ethylene glycol) blends with 45S5 bioactive glass particles. Mater. Lett. 205, 257–260. https://doi.org/10.1016/J.MATLET.2017.06.096.

Hong, X., Edirisinghe, M., Mahalingam, S., 2016. Beads, beaded-fibres and fibres: tailoring the morphology of Poly(Caprolactone) using pressurised gyration. Mater. Sci. Eng. C 69, 1373–1382. https://doi.org/10.1016/J.MSEC.2016.07.071.

Jaiswal, A.K., Chhabra, H., Kadam, S.S., Londhe, K., Soni, V.P., Bellare, J.R., 2013. Hardystonite improves biocompatibility and strength of electrospun polycaprolactone nanofibers over hydroxyapatite: a comparative study. Mater. Sci. Eng. C 33, 2926–2936. https://doi.org/10.1016/J.MSEC.2013.03.020.

Jirkovec, R., Holec, P., Hauzerova, S., Samkova, A., Kalous, T., Chvojka, J., 2021. Preparation of a composite scaffold from poly-caprolactone and hydroxyapatite particles by means of alternating current electrospinning. ACS Omega 6, 9234–9242. https://doi.org/10.1021/ACSOMEGA.1C00644.

Jones, J.R., 2013. Review of bioactive glass: from hench to hybrids. Acta Biomater. 9, 4457–4486. https://doi.org/10.1016/J.ACTBIO.2012.08.023.

Jones, J.R., Gentleman, E., Polak, J., 2007. Bioactive glass scaffolds for bone regeneration. Elements 3, 393–399. https://doi.org/10.2113/GSELEMENTS.3.6.393.

Joseph, B., Augustine, R., Kalarikkal, N., Thomas, S., Seantier, B., Grohens, Y., 2019. Recent advances in electrospun polycaprolactone based scaffolds for wound healing and skin bioengineering applications. Mater. Today Commun. 19, 319–335. https://doi.org/10.1016/J.MTCOMM.2019.02.009.

Jun, I., Han, H.S., Edwards, J.R., Jeon, H., 2018. Electrospun fibrous scaffolds for tissue engineering: viewpoints on architecture and fabrication. Int. J. Mol. Sci. 19, 745. https://doi.org/10.3390/IJMS19030745.

Kargozar, S., Milan, P.B., Amoupour, M., Kermani, F., Gorgani, S., Nazarnezhad, S., Hooshmand, S., Baino, F., 2022. Osteogenic potential of magnesium (Mg)-Doped multicomponent bioactive glass: in vitro and in vivo animal studies. Materials 15. https://doi.org/10.3390/MA15010318, 2022, 15.

Kaur, G., Pandey, O.P., Singh, K., Homa, D., Scott, B., Pickrell, G., 2014. A review of bioactive glasses: their structure, properties, fabrication and apatite formation. J. Biomed. Mater. Res. 102, 254–274. https://doi.org/10.1002/JBM.A.34690.

Keirouz, A., Wang, Z., Reddy, V.S., Nagy, Z.K., Vass, P., Buzgo, M., Ramakrishna, S., Radacsi, N., 2023. The history of electrospinning: past, present, and future developments. Adv. Mater. Technol. 8, 2201723. https://doi.org/10.1002/ADMT.202201723.

Kim, C.H., Khil, M.S., Kim, H.Y., Lee, H.U., Jahng, K.Y., 2006. An improved hydrophilicity via electrospinning for enhanced cell attachment and proliferation. J. Biomed. Mater. Res. B Appl. Biomater. 78, 283–290. https://doi.org/10.1002/JBM.B.30484.

Kim, H.H., Kim, M.J., Ryu, S.J., Ki, C.S., Park, Y.H., 2016. Effect of fiber diameter on surface morphology, mechanical property, and cell behavior of electrospun Poly (ε-Caprolactone) mat. Fibers Polym. 17 (7), 1033–1042. https://doi.org/10.1007/S12221-016-6350-X, 2016, 17.

Konyalı, R., Deliormanlı, A.M., 2019. Preparation and mineralization of 13-93 bioactive glass-containing electrospun poly-epsilon-caprolactone composite nanofibrous mats. J. Thermoplast. Compos. Mater. 32, 690–709. https://doi.org/10.1177/0892705718772889.

Kouhi, M., Morshed, M., Varshosaz, J., Fathi, M.H., 2013. Poly (ε-Caprolactone) incorporated bioactive glass nanoparticles and simvastatin nanocomposite nanofibers: preparation, characterization and in vitro drug release for bone regeneration applications. Chem. Eng. J. 228, 1057–1065. https://doi.org/10.1016/j.cej.2013.05.091.

Lindfors, N.C., Hyvönen, P., Nyyssönen, M., Kirjavainen, M., Kankare, J., Gullichsen, E., Salo, J., 2010. Bioactive glass S53P4 as bone graft substitute in treatment of osteomyelitis. Bone 47, 212–218. https://doi.org/10.1016/J.BONE.2010.05.030.

Liverani, L., Lacina, J., Roether, J.A., Boccardi, E., Killian, M.S., Schmuki, P., Schubert, D.W., Boccaccini, A.R., 2018. Incorporation of bioactive glass nanoparticles in electrospun PCL/chitosan fibers by using benign solvents. Bioact. Mater. 3, 55–63. https://doi.org/10.1016/J.BIOACTMAT.2017.05.003.

Liverani, L., Liguori, A., Zezza, P., Gualandi, C., Toselli, M., Boccaccini, A.R., Focarete, M.L., 2021. Nanocomposite electrospun fibers of Poly(ε-Caprolactone)/Bioactive glass with shape memory properties. Bioact. Mater. 11, 230. https://doi.org/10.1016/J.BIOACTMAT.2021.09.020.

Lu, H., Zhang, T., Wang, X.P., Fang, Q.F., 2008. Electrospun submicron bioactive glass fibers for bone tissue scaffold. J. Mater. Sci. Mater. Med. 20 (3), 793–798. https://doi.org/10.1007/S10856-008-3649-1, 2008, 20.

Luginina, M., Schuhladen, K., Orrú, R., Cao, G., Boccaccini, A.R., Liverani, L., 2020. Electrospun PCL/PGS composite fibers incorporating bioactive glass particles for soft tissue engineering applications. Nanomaterials 10. https://doi.org/10.3390/NANO10050978, 2020, 10.

Mecca, F.G., Bellucci, D., Cannillo, V., 2023. Effect of thermal treatments and ion substitution on sintering and crystallization of bioactive glasses: a review. Materials 16. https://doi.org/10.3390/MA16134651, 2023, 16.

Mecca, F.G., Muniz, N.O., Bellucci, D., Legallais, C., Baudequin, T., Cannillo, V., 2025. Inclusion of Magnesium- and strontium-enriched bioactive glass into electrospun PCL scaffolds for tissue regeneration. Polymers 17. https://doi.org/10.3390/POLYM17111555, 2025, 17.

Meng, J., Yang, G., Liu, L., Song, Y., Jiang, L., Wang, S., 2017. Cell adhesive spectra along surface wettability gradient from super-hydrophilicity to superhydrophobicity. Sci. China Chem. 60 (5), 614–620. https://doi.org/10.1007/s11426-016-9031-8, 2017, 60.

Moghanian, A., Dehghan Mehrjardi, L., Safaee, S., 2025. Ion substitution in bioactive glass: a comprehensive review of structural modifications and functional effects. Next Mater. 8, 100598. https://doi.org/10.1016/J.NXMATE.2025.100598.

Moghanian, A., Firoozi, S., Tahriri, M., 2017. Characterization, in vitro bioactivity and biological studies of sol-gel synthesized SrO substituted 58S bioactive glass. Ceram. Int. 43, 14880–14890. https://doi.org/10.1016/J.CERAMINT.2017.08.004.

Moura, D., Souza, M.T., Liverani, L., Rella, G., Luz, G.M., Mano, J.F., Boccaccini, A.R., 2017. Development of a bioactive glass-polymer composite for wound healing applications. Mater. Sci. Eng. C 76, 224–232. https://doi.org/10.1016/J.MSEC.2017.03.037.

Nagrath, M., Alhalawani, A., Rahimnejad Yazdi, A., Towler, M.R., 2019. Bioactive glass fiber fabrication via a combination of sol-gel process with electro-spinning technique. Mater. Sci. Eng. C 101, 521–538. https://doi.org/10.1016/J.MSEC.2019.04.003.

Percival, M., 1999. Bone health & osteoporosis. Appl. Nutr. Sci. Rep. 5.

Piatti, E., Miola, M., Liverani, L., Verné, E., Boccaccini, A.R., 2023. Poly (ε-Caprolactone)/Bioactive glass composite electrospun fibers for tissue engineering applications. J. Biomed. Mater. Res. 111, 1692–1709. https://doi.org/10.1002/JBM.A.37578.

Rabiee, S.M., Nazparvar, N., Azizian, M., Vashaee, D., Tayebi, L., 2015. Effect of ion substitution on properties of bioactive glasses: a review. Ceram. Int. 41, 7241–7251. https://doi.org/10.1016/J.CERAMINT.2015.02.140.

Sattary, M., Rafienia, M., Khorasani, M.T., Salehi, H., 2019. The effect of collector type on the physical, chemical, and biological properties of Polycaprolactone/gelatin/nano-hydroxyapatite electrospun scaffold. J. Biomed. Mater. Res. B Appl. Biomater. 107, 933–950. https://doi.org/10.1002/JBM.B.34188.

Sergi, R., Bellucci, D., Salvatori, R., Anesi, A., Cannillo, V., 2020. A novel bioactive glass containing therapeutic ions with enhanced biocompatibility. Materials 13, 1–16. https://doi.org/10.3390/MA13204600, 2020, 13.

Serio, F., Miola, M., Vernè, E., Pisignano, D., Boccaccini, A.R., Liverani, L., 2019. Electrospun filaments embedding bioactive glass particles with ion release and enhanced mineralization. Nanomaterials 9, 182. https://doi.org/10.3390/nano9020182.

Shams, M., Karimi, M., Ghollasi, M., Nezafati, N., Salimi, A., 2018. Electrospun Poly-l-Lactic acid nanofibers decorated with melt-derived S53P4 bioactive glass nanoparticles: the effect of nanoparticles on proliferation and osteogenic differentiation of human bone marrow mesenchymal stem cells in vitro. Ceram. Int. 44, 20211–20219. https://doi.org/10.1016/J.CERAMINT.2018.08.005.

Tabia, Z., Akhtach, S., Bricha, M., El Mabrouk, K., 2021. Tailoring the biodegradability and bioactivity of green-electrospun polycaprolactone fibers by incorporation of bioactive glass nanoparticles for guided bone regeneration. Eur. Polym. J. 161, 110841. https://doi.org/10.1016/J.EURPOLYMJ.2021.110841.

Tiyek, I., Gunduz, A., Yalcinkaya, F., Chaloupek, J., 2019. Influence of electrospinning parameters on the hydrophilicity of electrospun polycaprolactone nanofibres. J. Nanosci. Nanotechnol. 19, 7251–7260. https://doi.org/10.1166/JNN.2019.16605.

Wei, S., Jian, C., Xu, F., Bao, T., Lan, S., Wu, G., Qi, B.W., Bai, Z., Yu, A., 2018. Vancomycin–impregnated electrospun polycaprolactone (PCL) membrane for the treatment of infected bone defects: an animal study. J. Biomater. Appl. 32, 1187–1196. https://doi.org/10.1177/0885328218754462.

Wong, S.C., Baji, A., Leng, S., 2008. Effect of fiber diameter on tensile properties of electrospun poly(ε-caprolactone). Polymer (Guildf.) 49, 4713–4722. https://doi.org/10.1016/J.POLYMER.2008.08.022.

Woodruff, M.A., Hutmacher, D.W., 2010. The return of a forgotten polymer—polycaprolactone in the 21st century. Prog. Polym. Sci. 35, 1217–1256. https://doi.org/10.1016/J.PROGPOLYMSCI.2010.04.002.

Yaseri, R., Fadaie, M., Mirzaei, E., Samadian, H., Ebrahiminezhad, A., 2023. Surface modification of polycaprolactone nanofibers through hydrolysis and aminolysis: a comparative study on structural characteristics, mechanical properties, and cellular performance. Sci. Rep. 13 (1), 9434. https://doi.org/10.1038/s41598-023-36563-w, 2023, 13.

Zreiqat, H., Howlett, C.R., Zannettino, A., Evans, P., Schulze-Tanzil, G., Knabe, C., Shakibaei, M., 2002. Mechanisms of magnesium-stimulated adhesion of osteoblastic cells to commonly used orthopaedic implants. J. Biomed. Mater. Res. 62, 175–184. https://doi.org/10.1002/JBM.10270.